Original Article

Latin American Journal of Solids and Structures

www.lajss.org

Statistics of the Pareto front in Multi-objective Optimization under Uncertainties

Abstract

In this paper we address an innovative approach to determine the mean and a confidence interval for a set of objects analogous to curves and surfaces. The approach is based on the determination of the most representative member of the family by minimizing a Hausdorff distance. This method is applied to the analysis of uncertain Pareto frontiers in multi-objective optimization (MOO). The determination of the Pareto front of deterministic MOO is carried by minimizing the hypervolume contained between the front and the utopia point. We give some examples and we apply the approach to a truss-like structure for which conflicting objective functions such as the structure mass and the maximum displacement are both to be minimized.

Keywords

Uncertainty, Multi-Objective Optimization, Pareto Front, Random system, Hypersurface, Hypervolume

Mohamed Bassi[a]
Eduardo Souza de Cursi[b]*
Emmanuel Pagnacco[b]
Rachid Ellaia[a]

[a] LERMA, Mohammed V University in Rabat, Mohammadia School of Engineers, Rabat, BP 765, Ibn Sina avenue, Agdal, Morocco. E-mail: bassi.mohamed@gmail.com, ellaia@emi.ac.ma

[b] LMN, EA 3828, INSA de Rouen-Normandie, BP 8, 76801 Saint-Etienne du Rouvray, France. E-mail: souza@insa-rouen.fr, emmanuel.Pagnacco@insa-rouen.fr

*Corresponding author

http://dx.doi.org/10.1590/1679-78255018

Received April 06, 2018
In revised form September 08, 2018
Accepted September 19, 2018
Available online September 27, 2018

1 INTRODUCTION

In real-life situations, it is frequent to consider contradictory objectives to be satisfied simultaneously in order to furnish an acceptable solution belonging to a set of possible choices. For instance, in Engineering, it is usual to look for solutions that maximize the performance while minimizing the cost – what is generally contradictory. A consumer chooses the best bundle of goods that he can afford but looks for the minimal expenses, while a producer maximizes his income and minimizes both production time and total cost (Varian 2006, Varian 2009 and Mankiw 2011). Traders seek for investments making the expected portfolio returns as high as possible with the lowest risk possible (Hurson and Zopounidis 1997, Zopounidis 1999, Pätäri et al. 2018 and Craven and Islam 2005). In such a situation, compromises must be determined between the objectives – it is usual to look for the Pareto frontier associated to the multi-objective problem, which synthetizes the possible compromises and trade-offs between the objectives.

Multi-objective optimization (MOO) is deeply applied to furnish more realistic solutions to improve economic activity or industrial process (Amodeo et al. 2007 and Ivanov and Ray 2014). In addition, real problems are also characterized by uncertainty: in practice, parameters defining objectives and constraints may be subjected to variability or simply badly known. Thus, considering uncertainty becomes essential and we may find in the literature many works devoted to uncertainties in multi-objective optimization. For instance, in the field of economics, stochastic dominance has been introduced (Hadar and Russell 1969, Bawa 1975, Bawa and Goroff 1983) and is widely exploited in Economics, Finance and Social Sciences (see, for instance, a few among many works: Ji and Lejeune 2018, Light 2018, Yager 2018). Another approach often found in the literature concerns the determination of robust solutions, *id est*, solutions remaining stable for a given range or known scenarios of perturbation (see, for instance, a few among many works: Navabi and Mirzaei 2017, Bachur et al. 2017, Xidonas et al. 2017, Moreira et al. 2016).

The efforts to consider uncertainty in optimization have a long history (Sahinidis 2004), but it is rare to find works concerning statistics of the Pareto frontier, such as its mean, its variance or the determination of a confidence interval. Indeed, under uncertainty, Pareto frontier becomes uncertain and, when the uncertainties are modeled as

random variables, Pareto frontier becomes stochastic, so that we may look for its mean, variance and a confidence interval. Although natural, such an analysis appears as difficulty, since a Pareto frontier is an object belonging to an infinite dimensional vector space: for instance, when considering a bi-objective problem, the Pareto frontier is, in general, a curve in $\mathbb{R}^2$, which must be described by a vector map or an algebraic equation, *id est*, a vector function associating an interval $I \subset \mathbb{R}$ to a set of points in $\mathbb{R}^2$ ($I \ni t \to x(t) \in \mathbb{R}^2$) on an algebraic equation $\phi(x) = 0\,, x \in S$. A first approximation may consider the Pareto frontier as a cloud of points, but even in this case, difficulties arise, since each point is a variate from a distribution dependent on a parameter $t \in [0,1]$ and the value of t associated to each point is unknown – thus, the evaluation of statistics of the points request a previous procedure for the indexation of the points by t, what remains arbitrary. In this paper, we address this difficulty by an alternative approach, by considering that the median object is the most representative one in the family. This approach allows considering random objects that can be modeled by continuous geometric forms instead of a cloud of a data points. The approach is applied to Pareto frontiers, which are determined by the variational approach introduced in (Zidani et al. 2013, Souza de Cursi 2015) to solve deterministic MOO problems and that leads to the determination of Pareto frontier by minimizing a hypervolume, but other methods of determination may be used instead.

In section 2, we illustrate the difficulty about the determination of statistics of families of curves and the proposed approach. The rest of the paper is organized as follows. In section 3, the mathematical model of deterministic multi-objective optimization problems is presented, and then uncertainties are introduced in section 4 for the MOO problems with constraints. In section 5 we explain the process we follow to quantify the uncertainties, and how the link is established between Statistics and Geometry. Three academic problems are solved in section 6 in both deterministic and uncertain cases before to study a 5-bar truss structure problem in section 7. In these one two exogenous variables are made random. At last, a summary concludes this paper in section 8.

2 STATISTICS OF CURVES

In this section we illustrate the difficulties in the determination of statistics of families of curves and the proposed approach. Analogous difficulties arise in higher dimensional situations.

As previously observed, a curve in the plane is a set of points which may be described by an algebraic equation $\phi(\boldsymbol{x}) = 0, \boldsymbol{x} \in S$ or a map $\boldsymbol{x}: I \to \mathbb{R}^2$, where $I = (a,b) \subset \mathbb{R}$. We are interested in the situation where the curve depends upon a random variable $\boldsymbol{Y} \in \mathbb{R}^m$: the equation becomes $\phi(\boldsymbol{x}|\boldsymbol{Y} = \boldsymbol{y}) = 0\,, \boldsymbol{x} \in S(\boldsymbol{y})$ and the map reads as $\boldsymbol{x}(t|\boldsymbol{y}): I(\boldsymbol{y}) \to \mathbb{R}^2$. For instance, let us consider the family defined by:

$$\phi(\boldsymbol{x}|y) = x_2 - y = 0, S(y) = \{x: |x_1| \le y\} \tag{1}$$

We have:

$$\boldsymbol{x}(t|y) = (t,y)\,, t \in [-y,y]. \tag{2}$$

Assume that $y \in [0,1]$ is uniformly distributed. The mean value of the parameter is $E(y) = 1/2$ and, for a given t, the mean value of $\boldsymbol{x}(t|y)$ is $E\big(\boldsymbol{x}(t|y)\big) = (t, (1+|t|)/2)$ (Notice that $x_2 \in (|t|, 1)$. As shown in Figure 1, the means evaluated by this way do not correspond to the family: in fact, they generate a curve similar to the envelope of the family.

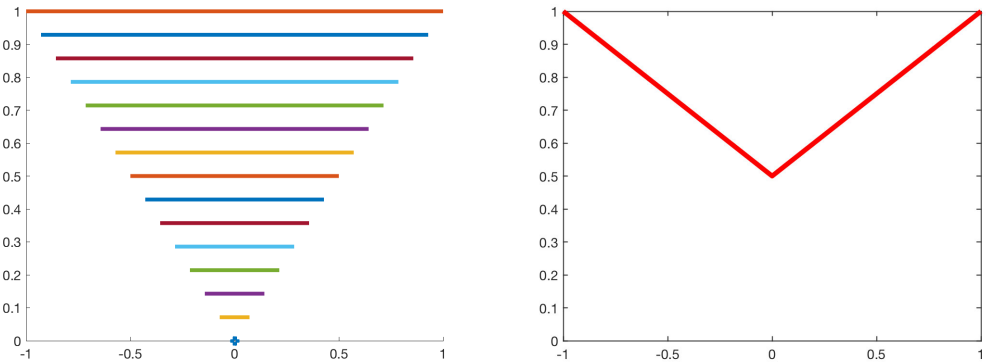

a) A family of curves b) The mean curve determined by examining the points

Figure 1: *An example where the mean generated by the points is not a member of the family*

As an alternative, we may adopt the standpoint presented in Croquet and Souza de Cursi (2010): let us introduce a fixed interval $J = [\alpha, \beta]$ and take $s \in J$ to describe all the curves of the family by using this variable. Here, $\boldsymbol{x}(s|y) = \big((2(s-\alpha) - (\beta-\alpha))y/(\beta-\alpha), y\big)\,, s \in [\alpha, \beta]$. Then, assuming regularity, we determine the expansion of $\boldsymbol{x}(s|y)$ in a convenient Hilbert basis and the mean of the coefficients:

$$\boldsymbol{x}(s|y) = \sum_{i=1}^{+\infty} \boldsymbol{x}_i(y)\varphi_i(s) \;\Rightarrow\; E\big(\boldsymbol{x}(s|y)\big) = \sum_{i=1}^{+\infty} E\big(\boldsymbol{x}_i(y)\big)\varphi_i(s)\,. \tag{3}$$

In this simple example, we may use a polynomial basis and we obtain:

$$E\big(\boldsymbol{x}(s|y)\big) = \big((2(s-\alpha) - (\beta-\alpha))/(2(\beta-\alpha)), 1/2\big)\,, s \in [\alpha, \beta] \tag{4}$$

so that the mean is a member of the family. Nevertheless, the approach introduced by Croquet and Souza de Cursi (2010) requests that the family is composed of parameterized curves. If the parameterization is missing, this method cannot be applied – it is necessary to determine a parameterization previously. In this work, we examine an alternative approach which may be applied without parameterization: we look for one of the elements of the family having a median position, *id est*, for a member of the family which occupies a central position and may be considered as a good representative of the family. In such a case, we look for the element of the family which is the nearest one for all the others. This is performed by minimizing the distance between nonparameterized curves – we use the Hausdorff distance (HD) defined in equation (17). Figure 2 shows the obtained result when this method is applied to the previous example.

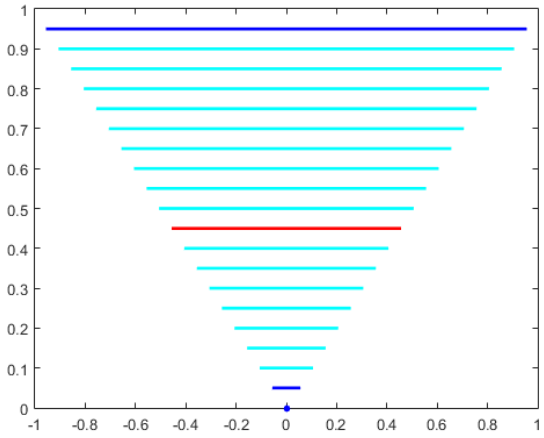

Figure 2: *The median curve (red) and the curves defining the "confidence interval" (cyan) are members of the family*

Once the median curve is determined, we may look for a "confidence interval" by finding a region including the mean curve and containing a given percentage of the family: usually, confidence intervals use a parameter $\boldsymbol{\alpha}$ – the risk – and a confidence level $\mathbf{1} - \boldsymbol{\alpha}$. For instance, we may look for a "confidence interval" having a level **90** % (thus, $\boldsymbol{\alpha} = \mathbf{10}$ %) by finding a region containing the 90% members of the family which are closer to the median curve, as shown in Figure 2. More generally, the difficulty exposed concerns the determination of the mean or the median of families of curves. Let us illustrate the situation by considering different families of random curves.

2.1 A family of random circles

Let us consider a family of circles having a random radius and a random initial phase:

$$\begin{cases} x(t) = r * \cos(t+\alpha) \\ y(t) = r * \sin(t+\alpha) \end{cases} \tag{5}$$

with $t \in [0,2\pi]$, r is uniformly distributed on [1,3] and α is uniformly distributed on $[0,2\pi]$. If the pointwise mean is considered, we have $E\big(x(t)\big) = E\big(y(t)\big) = 0$, so that the mean is a point: the origin (0,0). However, the expected mean is a circle of radius $r = 2$. In practical situations, we have a finite sample of the family: for instance, let us consider a sample of ns circles from this family, shown in Figure 3. We represent the empirical pointwise mean of the sample in black and the median curve in red, for samples of $ns = 100$ (at left) and $ns = 1000$ (at right). Green circles correspond to the confidence interval with a risk $\alpha = 10\%$. Blue circles lay outside the confidence interval – as expected these are the outermost ones, symmetrically distributed on the interior and exterior boundaries of the family – the blue circles represent 10% of the sample. Analogously, the pointwise mean furnishes a small circle near the origin, with a radius that goes to zero when the size of the sample increases.

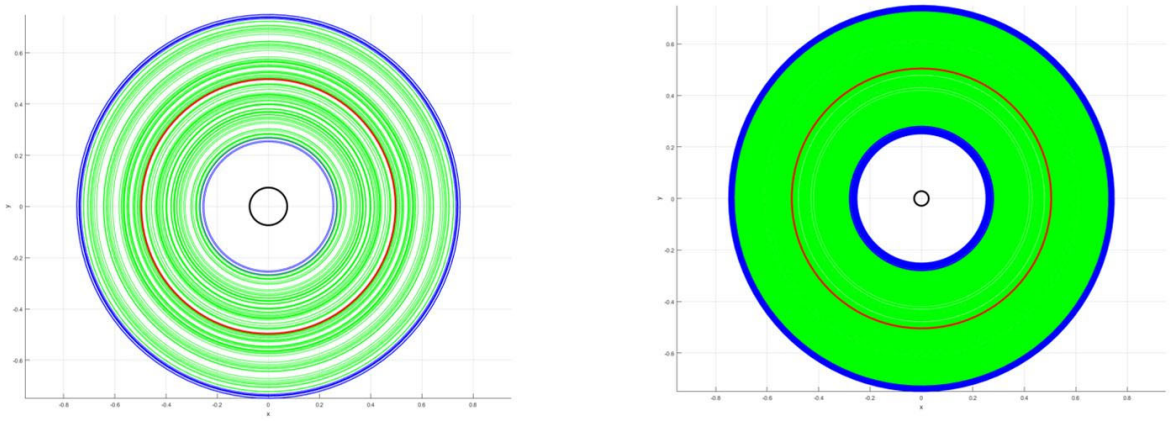

a) $ns = 100$ b) $ns = 1000$

Figure 3: *The pointwise mean circle (in black) in near the origin, the median generated by examining the Hausdorff distances (in red) is central. green circles correspond to the confidence interval*

2.2 A family of random arcs of circles

Let us consider a family of random arcs of circles generated as follows:

$$\begin{cases} x(t) = a + \cos(t + \alpha) \\ y(t) = b + \sin(t + \alpha) \end{cases} \tag{6}$$

where $t \in [0\,, \pi/4\,]$, α is uniformly distributed on $[0,2\pi]$, a and b are uniformly distributed on $[-1,1]$. For independent variables, $E\big(x(t)\big) = E\big(y(t)\big) = 0$.

As previously done with circles, we consider samples of $ns = 100$ (at left in Figure 4) and $ns = 1000$ (at right in Figure 4). Green arcs lay in the confidence interval with a risk $\alpha = 10\%$. Blue segments are outside this confidence interval – as expected these are the outermost ones. As in the preceding example, the blue curves represent 10% of the sample and the pointwise mean furnishes a small curve near the origin, that goes to zero when the size of the sample increases.

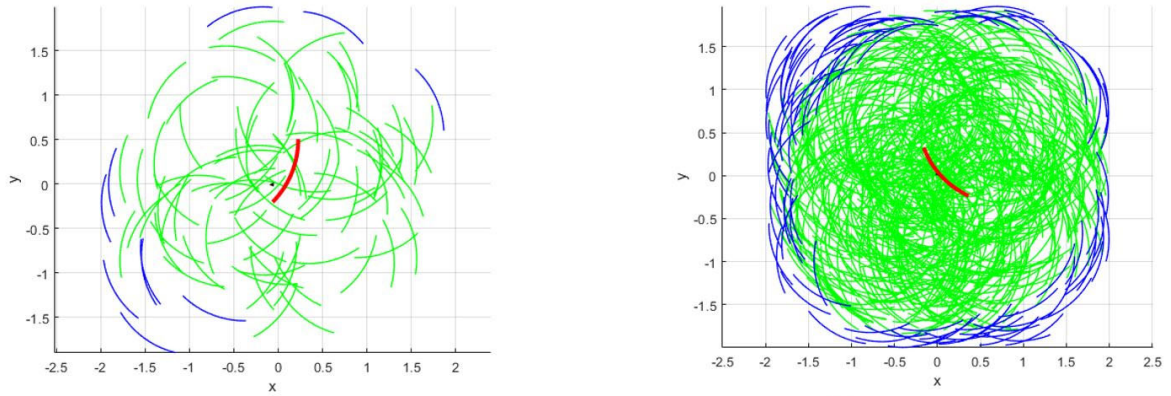

a) $ns = 100$ b) $ns = 1000$

Figure 4: *The pointwise mean arc of circle (in black) reduces to a point, the median one generated by examining the Hausdorff distances (in red), and the confidence interval (green arcs of circle)*

2.3 A Van der Pol oscillator with a random initial position

As a third example, we consider a Van der Pol oscillator

$$\ddot{x} = -x + (a - x^2)\dot{x}\,, x(0) = x_0\,; \dot{x}(0) = 0\,. \tag{7}$$

We consider $a = 0.5$ and $a = 1$, x_0 is uniformly distributed on $[0,1]$. A sample of $ns = 100$ curves in the phase space $(x, \dot{x})$ is generated by simulating the motion on the time interval $(0, 10)$. As in the previous examples, we

exhibit the statistical characteristics of interest from this family. In this case again, the mean curve is not a trajectory of the system, while the median is a member of the family. The results are displayed in Figure 5 considering the confidence interval at the same level used before. It is interesting to notice that, in this case, the confidence interval may be considered as unilateral.

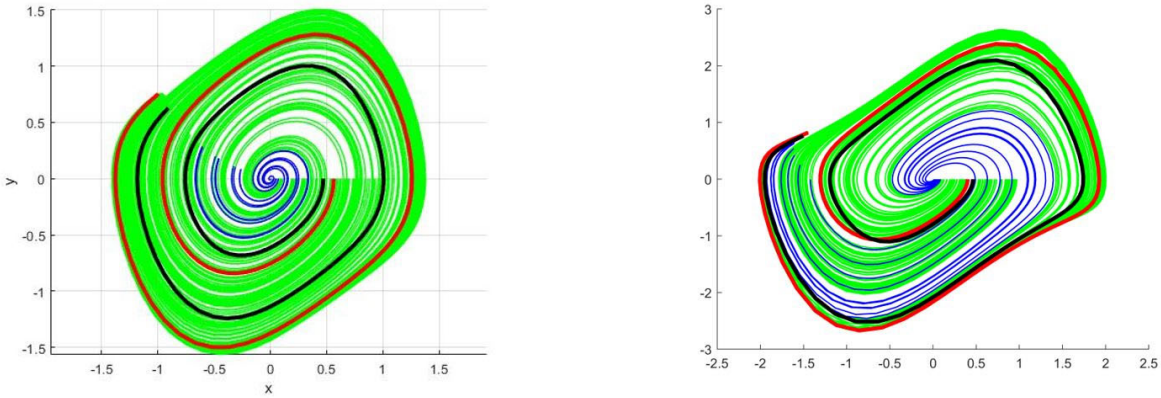

Figure 5: *The results for the Van der Pol oscillator with random initial position: pointwise mean (black curve) is not a trajectory, while the median (red curve) is a feasible trajectory. Green curves correspond to the confidence interval.*

2.4 A Duffing oscillator with random parameters

A last example is given by the Duffing oscillator:

$$\ddot{x} = -ax - bx^3 \, , x(0) = x_0 \, ; \dot{x}(0) = 1 \, . \tag{8}$$

We consider a is uniformly distributed on $[0.5, 1.5]$, and b uniformly distributed on $[0.1, 0.2]$. The results are exhibited in Figure 6. We observe that the pointwise mean does not correspond to a trajectory in the phase space, while the median is a feasible trajectory.

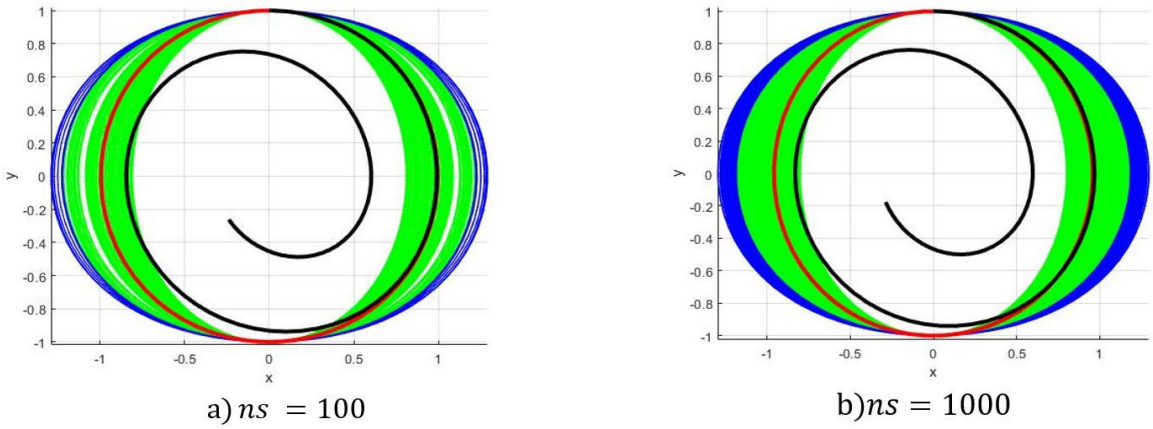

Figure 6: *Results for the Duffing oscillator with random parameters: pointwise mean (black curve) is not a trajectory, while the median (red curve) is a feasible trajectory. Green curves correspond to the confidence interval.*

As established in the preceding examples, this approach is effective to furnish the median and, then, to generate a confidence interval of a family of curves, so that we may consider its application to the determination of the mean and a confidence interval of Pareto's fronts. In the sequel, this method is used in order to quantify uncertainties in MOO problems. Initially (section 6), it is applied to three classical test problems and then (section 7), to the analysis of a 5 bar truss structure MOO problem.

3 DETERMINISTIC MULTIOBJECTIVE OPTIMIZATION

As usual, a standard MOO problem is modeled with a system of equalities and inequalities equations as follows:

$$\begin{cases} \underset{\boldsymbol{x}\in\mathbb{R}^d}{\text{Minimize}}\ \boldsymbol{f}(\boldsymbol{x}|\boldsymbol{y}) = (f_1(\boldsymbol{x}|\boldsymbol{y}), f_2(\boldsymbol{x}|\boldsymbol{y}), \dots, f_n(\boldsymbol{x}|\boldsymbol{y})) \\ \text{Subject to} \quad \begin{vmatrix} \boldsymbol{g}(\boldsymbol{x}|\boldsymbol{y}) = (g_1(\boldsymbol{x}|\boldsymbol{y}), \dots, g_p(\boldsymbol{x}|\boldsymbol{y})) \le \boldsymbol{0} \\ \boldsymbol{h}(\boldsymbol{x}|\boldsymbol{y}) = \left(h_1(\boldsymbol{x}|\boldsymbol{y}), \dots, h_k(\boldsymbol{x}|\boldsymbol{y})\right) = \boldsymbol{0} \\ \boldsymbol{x}_l \le \boldsymbol{x} \le \boldsymbol{x}_u \end{vmatrix} \end{cases} , (\boldsymbol{x}_l, \boldsymbol{x}_u) \in \mathbb{R}^d \times \mathbb{R}^d \tag{9}$$

or more simply:

$$\begin{cases} \underset{\boldsymbol{x}\in\mathbb{R}^d}{\text{Minimize}}\ \boldsymbol{f}(\boldsymbol{x}|\boldsymbol{y}) = (f_1(\boldsymbol{x}|\boldsymbol{y}), f_2(\boldsymbol{x}|\boldsymbol{y}), \dots, f_n(\boldsymbol{x}|\boldsymbol{y})) \\ \text{Subject to} \quad \begin{vmatrix} \boldsymbol{x} \in S_d \\ S_d \subset \mathbb{R}^d \end{vmatrix} \end{cases} \tag{10}$$

In these two systems:

- $f_1, f_2, \dots, f_n$ are the objective functions
- $g_1, g_2 \dots, g_p$ are the inequality constraints
- $h_1, h_2 \dots, h_k$ are the equality constraints
- $\boldsymbol{x} = (x_1, x_2, \dots, x_d)^{\mathrm{t}} \in \mathbb{R}^d$ is the decision variables vector
- $\boldsymbol{x_l}$ (resp. $\boldsymbol{x_u}$) is the lower boundary (resp. upper boundary)
- $\boldsymbol{y} = (y_1, y_2, \dots, y_m)^{\mathrm{t}} \in \mathbb{R}^m$ represents the values of the exogenous parameters
- S_n is the feasible space including all the constraints and boundaries above

Numerous methods can be used to solve deterministic MOO problems, such as the weighting method (Gass and Saaty 1955 and Zadeh 1963), the å-constraint method (Haimes et al. 1971), Geoffrion-Dyer-Feinberg Method (Geoffrion et al. 1972), the Keeney-Raiffa method (Keeney and Raiffa 1994) and more (see for instance: Miettinen 1999 and Collette and Siarry 2002) and in this work we use a variational method called here the Zidani-Souza's method that has been proposed by Zidani et al. (2013) and which is presented in the appendix A. It consists in minimizing the hypervolume between the Pareto front and the utopia point. In this method, the decision variables are developed in polynomials, what allows to get a piecewise continuous Pareto front.

4 MULTIOBJECTIVE OPTIMIZATION UNDER UNCERTAINTIES

To take the uncertainties into account, we introduce the random vector $\boldsymbol{Y}$ of exogenous variables, in replacement of the deterministic vector $\boldsymbol{y}$. As a consequence, both objective functions and constraints become random. In this case, equality and inequality constraints become probabilistic and the standard MOO problem becomes:

$$\begin{cases} \underset{\boldsymbol{x}\in\mathbb{R}^d}{\text{Minimize}}\ \boldsymbol{F}(\boldsymbol{x}|\boldsymbol{Y}) = (F_1(\boldsymbol{x}|\boldsymbol{Y}), F_2(\boldsymbol{x}|\boldsymbol{Y}), \dots, F_n(\boldsymbol{x}|\boldsymbol{Y})) \\ \text{Subject to} \quad \begin{vmatrix} \text{Prob}\left(\boldsymbol{G}(\boldsymbol{x}|\boldsymbol{Y}) = \left(G_1(\boldsymbol{x}|\boldsymbol{Y}), \dots, G_p(\boldsymbol{x}|\boldsymbol{Y})\right) \le \boldsymbol{0}\right) \ge \alpha \\ \text{Prob}\left(\boldsymbol{H}(\boldsymbol{x}|\boldsymbol{Y}) = \left(H_1(\boldsymbol{x}|\boldsymbol{Y}), \dots, H_k(\boldsymbol{x}|\boldsymbol{Y})\right) = \boldsymbol{0}\right) \ge \beta \\ \boldsymbol{x}_l \le \boldsymbol{x} \le \boldsymbol{x}_u \end{vmatrix} \end{cases} , (\boldsymbol{x}_l, \boldsymbol{x}_u) \in \mathbb{R}^d \times \mathbb{R}^d \tag{11}$$

where Prob is the probability operator, $\boldsymbol{Y}$ has a given joint probability distribution, and α and β are the reliability probabilities that are imposed by the decision maker. Then, each realization $\boldsymbol{y}_i = \left(y_{1,i}, y_{2,i}, \dots, y_{m,i}\right)^{\mathrm{t}}$ of $\boldsymbol{Y}$ leads to a unique deterministic MOO problem that generates a piecewise continuous Pareto front, and a sample $\{\boldsymbol{y}_1, \boldsymbol{y}_2, \dots, \boldsymbol{y}_{ns}\}$ of $\boldsymbol{Y}$ leads to ns distinct MOO problems and a set of ns different curves (or hypersurfaces).

As previously mentioned, the main goal of this work is to focus on uncertainties in MOO; more precisely, a link is established between Geometry and Statistics when the randomness of an exogenous variable lead to a set of Pareto fronts instead of one front. In fact, our objective is to evaluate statistical quantities, namely confidence intervals of a set from the single data furnished by the set itself, without the use of an external probability – they are generated by using "means" (or "medians"). Then, considering randomness on a MOO problem inputs, we explore the outputs, namely the trade-offs, and extract from the family its "median" and other "quantile curves", more generally the hypersurfaces that belong also to the same set. In other words, we search for a mean of a set of subjects that is *one of its members*.

5 IMPLEMENTATION

In practice, the approach under consideration is implemented as follows:

- A sample $\left\{\boldsymbol{y}_1, \boldsymbol{y}_2, \dots, \boldsymbol{y}_{ns}\right\}$ of the random vector $\boldsymbol{Y}$ is generated

• By using a Monte Carlo simulation, we get for each m-tuple $\boldsymbol{y}_i = \left(y_{i,1}, y_{i,2}, \dots, y_{i,m}\right)^{\mathrm{t}}$ such as $1 \leq i \leq ns$ a new MOO problem. In this work we focus on the bi-objective optimization problems with inequality constraints, then, theoretically, each value of the sample, leads to a new problem defined as follows:

$$\begin{cases} \underset{\boldsymbol{x}\in\mathbb{R}^d}{\text{Minimize}}\, \boldsymbol{f}_i(\boldsymbol{x}|\boldsymbol{y}_i) = \left(f_{1,i}(\boldsymbol{x}|\boldsymbol{y}_i), f_{2,i}(\boldsymbol{x}|\boldsymbol{y}_i)\right), i \in \{1,2,\dots,ns\} \\ \text{Subject to} \quad \left|\begin{array}{l} \text{Prob}\left(g(\boldsymbol{x}|\boldsymbol{y}_i) = \left(g_1(\boldsymbol{x}|\boldsymbol{y}_i), \dots, g_p(\boldsymbol{x}|\boldsymbol{y}_i)\right) \leq 0\right) \geq \alpha \\ \boldsymbol{x}_l \leq \boldsymbol{x} \leq \boldsymbol{x}_u \end{array}\right. , (\boldsymbol{x}_l, \boldsymbol{x}_u) \in \mathbb{R}^d \times \mathbb{R}^d \end{cases} \tag{12}$$

• Each problem is solved by using the Zidani-Souza's method and ns Pareto fronts denoted S_i^* are obtained.
• We compute the sum of the distances between each Pareto front and all the other ones:

$$D_i = \sum_{j=1}^{ns} d(S_i^*, S_j^*) \tag{13}$$

where $d\left(S_i^*, S_j^*\right)$ is a well-chosen distance.
• The mean Pareto front is defined as:

$$\bar{S} = S_k^* \quad \text{such as} \begin{cases} S_k^* \in \{S_1^*, S_2^*, \dots, S_{ns}^*\} \\ D_k = \min\, \{D_i |\, i \in [\![1, ns]\!]\} \end{cases} \tag{14}$$

• The $x\%$-quantile-hypersurfaces:

$$S_{x\%} = S_k^* \text{ such as } \begin{cases} S_k \in S \\ \text{Prob}(D \leq d_k) = x \end{cases} \tag{15}$$

where D is a random variable taking values in the resulting set $\{D_1, D_2, \dots, D_{ns}\}$.

In this work, we consider two distances:

1) The L^2 distance given by:

$$d\left(S_i^*, S_j^*\right) = \left\|F_i - F_j\right\|_2$$

$$= \sqrt{\int_x \left(f_{1,i}(\boldsymbol{x}|\boldsymbol{y}_i) - f_{1,j}\left(\boldsymbol{x}|\boldsymbol{y}_j\right)\right)^2 + \left(f_{2,i}(\boldsymbol{x}|\boldsymbol{y}_i) - f_{2,j}\left(\boldsymbol{x}|\boldsymbol{y}_j\right)\right)^2} \; ; \; (i,j) \in [\![1, ns]\!]^2 \tag{16}$$

2) The Hausdorff distance given by:

$$d_H\left(S_i^*, S_j^*\right) = \max\left\{\sup_{x\in S_i^*} \delta\left(x, S_j^*\right), \sup_{y\in S_j^*} \delta\left(y, S_i^*\right)\right\} \; ; \; (i,j) \in [\![1, ns]\!]^2 \tag{17}$$

where S_i^* and S_j^* are closed bounded non-empty subsets of the metric space $(\mathbb{R}^d, \delta)$.

In a first step, we considered both the distances: tests running with each one provided results that were compared and showed to be almost identical. Then, in a second step, we considered the single Hausdorff distance and a larger sample ($ns = 200$) to determine the quantities of interest.

6 TEST FUNCTIONS

In this section, three academic test functions are considered. All are solved as deterministic problems before uncertainties are considered. All the problems are bi-objective, involving constraints, as previously mentioned.

6.1 Binh and Korn function

The original problem is reported in Binh and Korn (1997) and is as follows:

$$\underset{\boldsymbol{x}\in\mathbb{R}^2}{\text{Minimize}} \begin{cases} f_1(\boldsymbol{x}) = f_1(x_1, x_2) = 4x_1^2 + 4x_2^2 \\ f_2(\boldsymbol{x}) = f_2(x_1, x_2) = (x_1 - 5)^2 + (x_2 - 5)^2 \end{cases}$$

$$\text{Such that} \begin{cases} (x_1 - 5)^2 + {x_2}^2 \leq 25 \\ (x_1 - 8)^2 + (x_2 + 3)^2 \geq 7.7 \\ 0 \leq x_1 \leq 5\,, 0 \leq x_2 \leq 3 \end{cases} \tag{18}$$

By applying Zidani-Souza's method of the appendix A, this problem is efficiently solved by expanding x_1 and x_2 as polynomials of degree 6, having their coefficients in $[-c_{max}, c_{max}] = [-10,10]$. The numerical results are as following:

$$\boldsymbol{x}_1^* = \underset{\boldsymbol{x} \in S_d}{\operatorname{argmin}} f_1(\boldsymbol{x}) = (0,0)^{\mathrm{t}}$$

$$\boldsymbol{x}_2^* = \underset{\boldsymbol{x} \in S_d}{\operatorname{argmin}} f_2(\boldsymbol{x}) = (5,3)^{\mathrm{t}}$$

$$\boldsymbol{f}_{utopia} = \left(f_1(\boldsymbol{x}_1^*), f_2(\boldsymbol{x}_2^*)\right)^{\mathrm{t}} = (0,4)^{\mathrm{t}}$$

$$A_{sol} = \int_{t\in[0,1]} \left\langle \mathrm{rot}\left(\boldsymbol{p}^*(t)\right) \middle| \nabla \boldsymbol{p}^*(t) \right\rangle \mathrm{d}t = 1431$$

$\langle . | . \rangle$ being the scalar product, $\mathrm{rot}\left(\boldsymbol{p}^*(.)\right)$ the rotational of $\boldsymbol{p}^*$and A_{sol} is the area (or hypervolume) that was minimized and that is bounded by the utopia point and the Pareto front given by $\boldsymbol{p}^* = (f_1^*, f_2^*)$.

The corresponding Pareto front is presented in Figure 7.

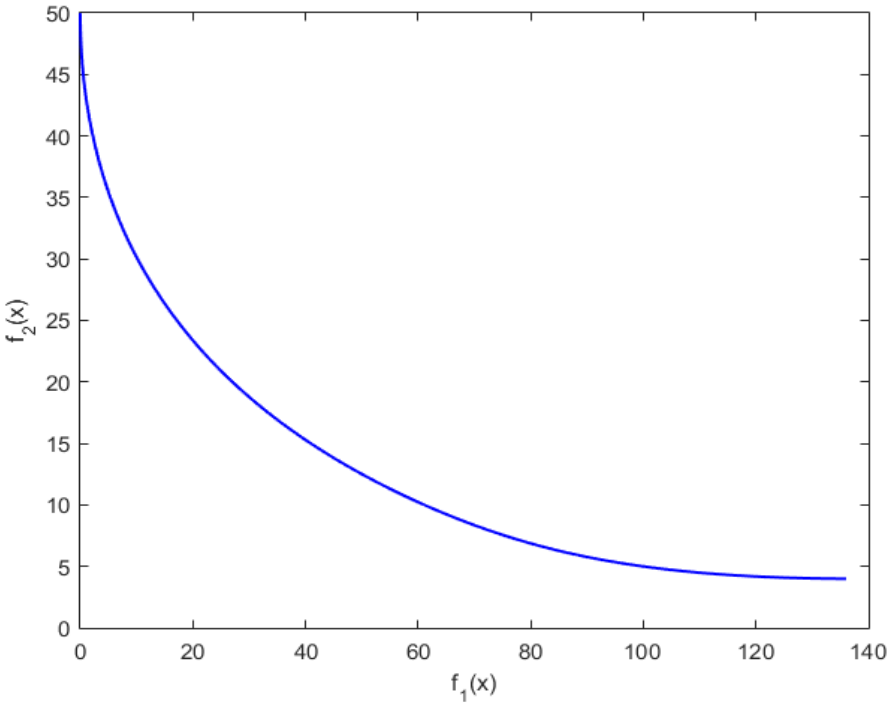

Figure 7: *Pareto front of the Binh and Korn test function*

To make the problem uncertain, we introduce randomness in the 2nd objective function by using two uncorrelated random variables ξ_1 and ξ_2 that are uniformly distributed on [0,1]:

$$\underset{\boldsymbol{x}\in\mathbb{R}^2}{\text{Minimize}} \begin{cases} f_1(\boldsymbol{x}) = 4(x_1 + \xi_1)^2 + 4(x_2 + \xi_2)^2 \\ f_2(\boldsymbol{x}) = (x_1 - 0.2\xi_1 - 5)^2 + (x_2 - 0.2\xi_2 - 5)^2 \end{cases}$$

$$\text{Such that } \begin{cases} (x_1 - 5)^2 + {x_2}^2 \leq 25 \\ (x_1 - 8)^2 + (x_2 + 3)^2 \geq 7.7 \\ 0 \leq x_1 \leq 5\,, 0 \leq x_2 \leq 3 \end{cases} \tag{19}$$

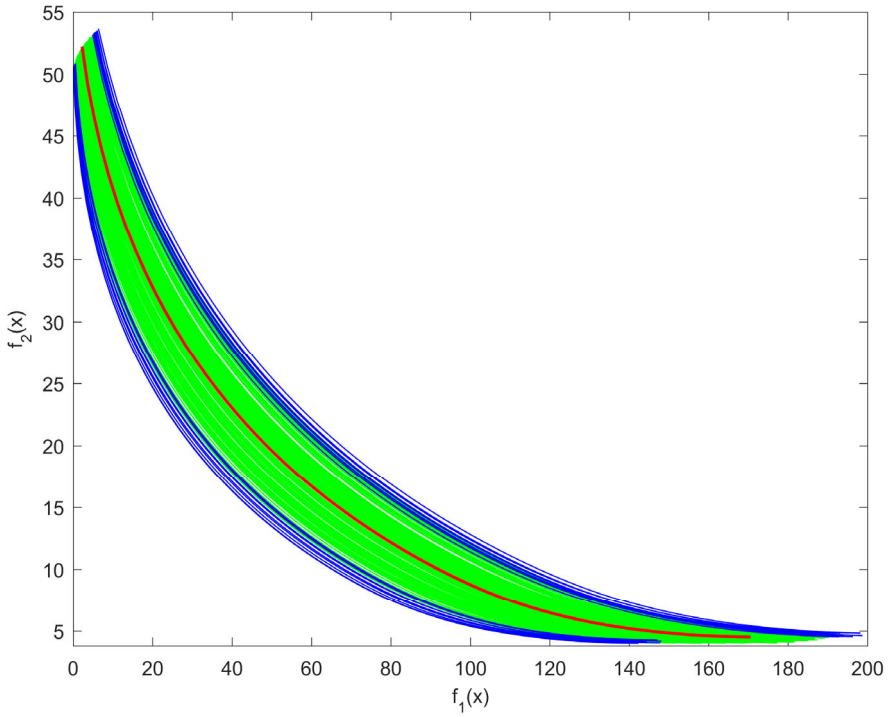

Figure 8: *Binh and Korn function under uncertainties for ns=200 sample size: the median Pareto front appears in red, the confidence interval in green and the Pareto fronts beyond the 90%-quantile in blue*

Since there are no uncertainties in constraints, they must be satisfied at a 100% level of probability for the problem solution. Figure 8 shows the 200 Pareto fronts obtained, with the mean front in red, the 180 nearest fronts to the mean in green and the 20 farthest ones - in the sense of Hausdorff's distance - in blue. Thus, the green curves correspond to the 90% closer to the median in the sense of Hausdorff's distance and may be considered as belonging to a confidence interval with risk $\text{ị} = 10\%$. We observe that, as expected, the median is a central curve and the curves laying outside the confidence interval are the outermost ones.

6.2 Fonseca and Fleming function

The Fonseca and Fleming problem (Fonseca and Fleming 1995) is:

$$\underset{\boldsymbol{x}\in\mathbb{R}^3}{\text{Minimize}} \begin{cases} f_1(\boldsymbol{x}) = 1 - \exp\left[-\sum_{i=1}^{3}\left(x_i - \frac{1}{\sqrt{3}}\right)^2\right] \\ f_2(\boldsymbol{x}) = 1 - \exp\left[-\sum_{i=1}^{3}\left(x_i + \frac{1}{\sqrt{3}}\right)^2\right] \end{cases} \tag{20}$$

$$\text{such that}: \; -4 \le x_i \le 4 \; ; \; i \in \{1,2,3\}$$

Here yet, polynomials of the 6th. degree with coefficients on $[-\mathrm{c}_{\max}, \mathrm{c}_{\max}] = [-10,10]$ are considered. The numerical results are the following, and the Pareto front is shown in Figure 9:

$$\boldsymbol{x}_1^* = \underset{\boldsymbol{x}\in S_d}{\operatorname{argmin}} f_1(\boldsymbol{x}) = \left(\frac{1}{\sqrt{3}}, \frac{1}{\sqrt{3}}, \frac{1}{\sqrt{3}}\right)^{\mathrm{t}}$$

$$\boldsymbol{x}_2^* = \underset{\boldsymbol{x}\in S_d}{\operatorname{argmin}} f_2(\boldsymbol{x}) = -\left(\frac{1}{\sqrt{3}}, \frac{1}{\sqrt{3}}, \frac{1}{\sqrt{3}}\right)^{\mathrm{t}}$$

$$\boldsymbol{f}_{utopia} = \left(f_1(\boldsymbol{x}_1^*), f_2(\boldsymbol{x}_2^*)\right)^{\mathrm{t}} = (0,0)^{\mathrm{t}}$$

$$A_{sol} = \int_{t\in[0,1]} \langle \mathrm{rot}(\boldsymbol{p}^*(t) | \nabla \boldsymbol{p}^*(t)) \rangle \mathrm{d}t = 0.6579$$

Three uncorrelated random variables ξ_1, ξ_2 and ξ_3 that are all uniformly distributed on [0,0.1] are added to this system in order to make it uncertain, then $ns = 200$ deterministic problems derived from the initial one are obtained as follows:

$$\underset{\boldsymbol{x}\in\mathbb{R}^3}{\text{Minimize}} \begin{cases} f_1(\boldsymbol{x}) = 1 - \exp\left[-\sum_{i=1}^{3}\left(x_i - \frac{1}{\sqrt{3}} + \xi_i\right)^2\right] \\ f_2(\boldsymbol{x}) = 1 - \exp\left[-\sum_{i=1}^{3}\left(x_i + \frac{1}{\sqrt{3}} - \xi_i\right)^2\right] \end{cases} \tag{21}$$

$$\text{such that}: \; -4 \leq x_i \leq 4 \; ; \; i \in \{1,2,3\}$$

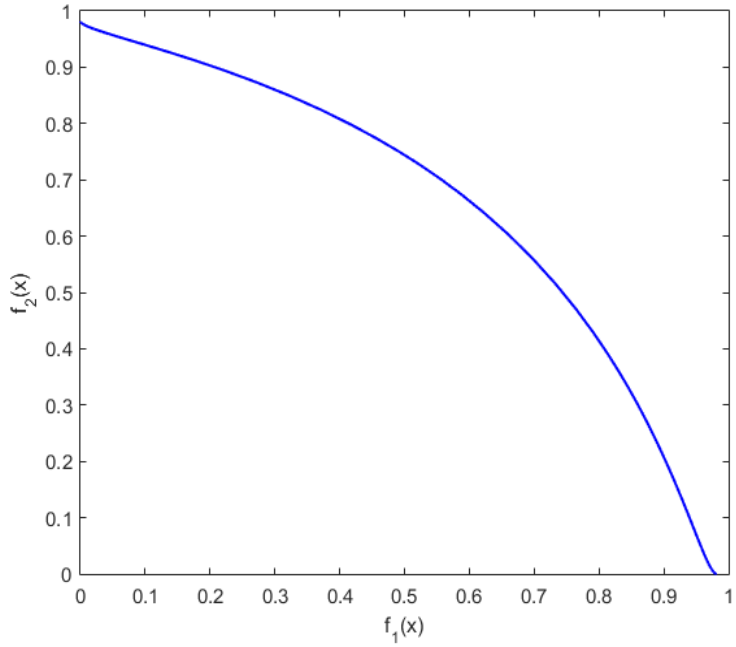

Figure 9: *Pareto front of the Fonseca and Fleming test function*

Figure 10 shows the 200 curves we get and the mean that minimizes both of the distances that we used is in the middle of the curves set as expected.

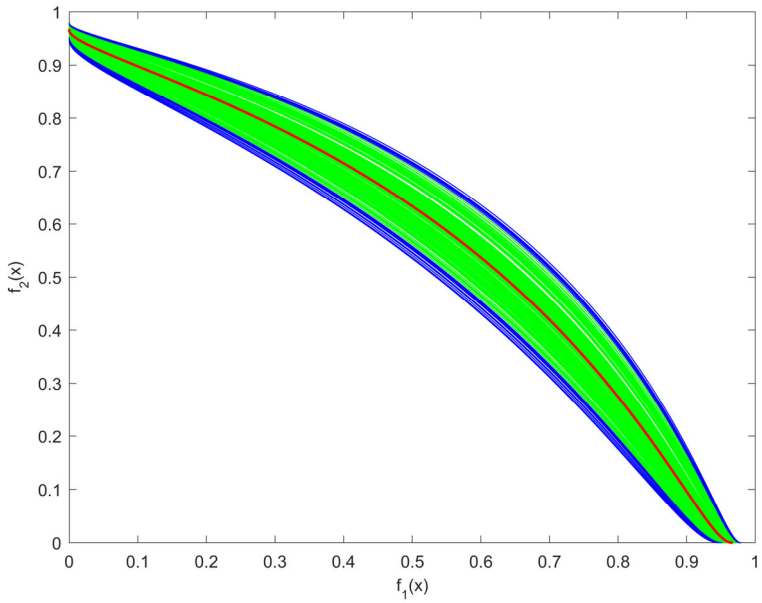

Figure 10: *Fonseca and Fleming under uncertainties for* $ns = 200$*: the median Pareto front appears in red, the confidence interval in green and the Pareto fronts beyond the 90%-quantile in blue*

In this case $f_2(f_1(\boldsymbol{x}))$ is a concave function, furthermore, all of the Pareto fronts ends are located together is a small region of space. In this case, the Hausdorff distance exhibits a larger variation in the middle of the family of curves, so that the curves beyond the 90%-quantile (in blue) appear more clearly when compared to the preceding situation. Notice that the median appears as a mean curve, in the center of the family.

6.3 Zitzler-Deb-Thiele's function 3 (ZDT3)

Let us consider the function g of $\boldsymbol{x} = (x_1, x_2, \dots, x_n)$ defined such as:

$$g(\boldsymbol{x}) = 1 + \frac{9}{n-1}\sum_{i=2}^{n} x_i \tag{22}$$

Then, the ZDT3 Problem, which is reported in Zitzler et al. (2000) reads as follows:

$$\underset{\boldsymbol{x}\in\mathbb{R}^n}{\text{Minimize}} \begin{cases} f_1(\boldsymbol{x}) = x_1 \\ f_2(\boldsymbol{x}) = 1 - \sqrt{\frac{f_1(\boldsymbol{x})}{g(\boldsymbol{x})}} - \left(\frac{f_1(\boldsymbol{x})}{g(\boldsymbol{x})}\right)\sin\left(10\pi f_1(\boldsymbol{x})\right) \\ 0 \le x_i \le 1 \; i \in \{1,2,\dots,n\} \end{cases} \tag{23}$$

Here we consider the case $n = 2$. The Pareto front of this problem is given in Figure 11.

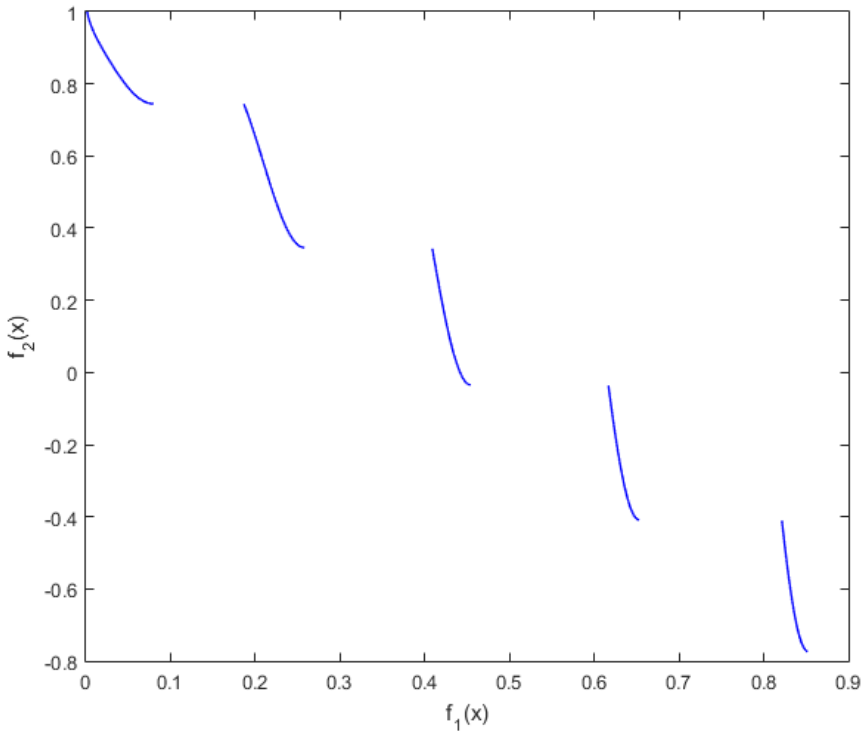

Figure 11: *Pareto front of the ZDT3 test function*

In order to make the problem uncertain, we introduce two uncorrelated random variables ξ_1 and ξ_2 that are uniformly distributed on [0,1] and on [−0.15,0.15], respectively. Then, we consider

$$\begin{cases} f_1(\boldsymbol{x}) = x_1 + \xi_1 \\ f_2(\boldsymbol{x}) = 1 + \xi_2 - \sqrt{\frac{f_1(\boldsymbol{x})}{g(\boldsymbol{x})}} - \left(\frac{f_1(\boldsymbol{x})}{g(\boldsymbol{x})}\right)\sin\left(10\pi f_1(\boldsymbol{x})\right) \end{cases} \tag{24}$$

In Figure 12, we exhibit the results obtained from a sample of ns = 200.

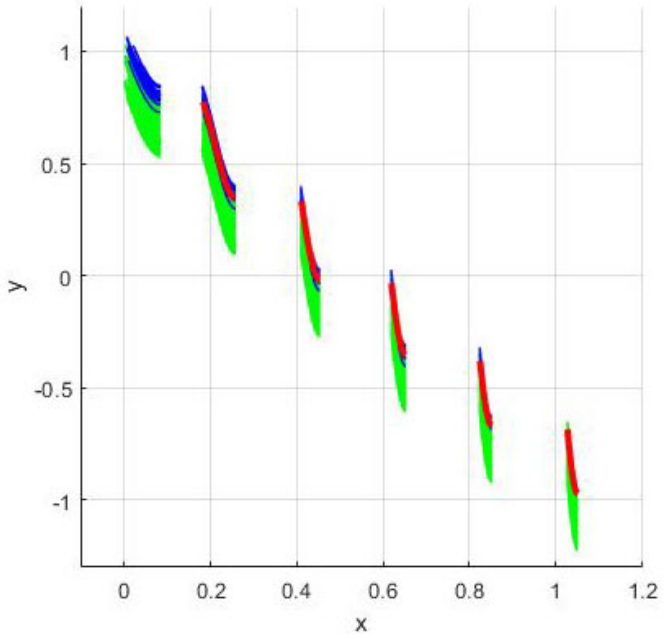

Figure 12: *Pareto fronts of the ZDT3 test function involving uncertainties: for* $ns = 200$*: the median Pareto front appears in red, the confidence interval in green and the Pareto fronts beyond the 90%-quantile in blue*

In this case, the Pareto's front is discontinuous. This fact makes that Hausdorff's distances between curves that seem close to the eye are, in fact, large in the sense of Hausdorff's distance. This fact is due to the fact that some parts of a curve may be isolated from the other curve, so that the distance of these points to the other one is large. For instance, let us consider the fronts shown in Fig. 13: the blue front may appear to the eye as being closer to the red one than the green front, but the respective Hausdorff's distances are 0.4132 and 0.1975, so that the green front is closer to the red one in the Hausdorff's sense. Observe that the red front has points which are far from the blue one.

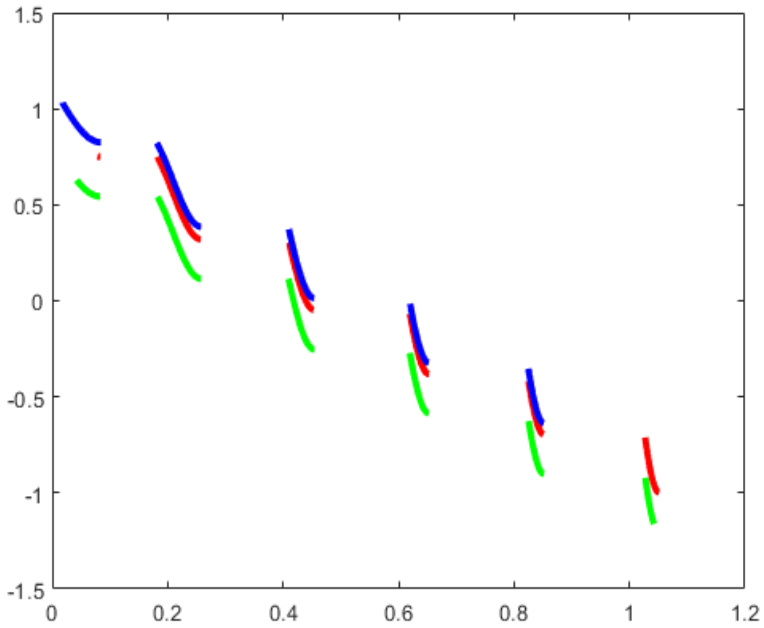

Figure 13: *The blue front may appear as closer to the median (in red) than the green one, but its Hausdorff's distance is the greatest one.*

An alternative consists in evaluating the distances only on the first 5 parts of the front (thus, in neglecting the last one). In this case, we obtain the result shown in Figure 14: in this case, the results better fit the eye's expectations, but the confidence interval appears as unilateral.

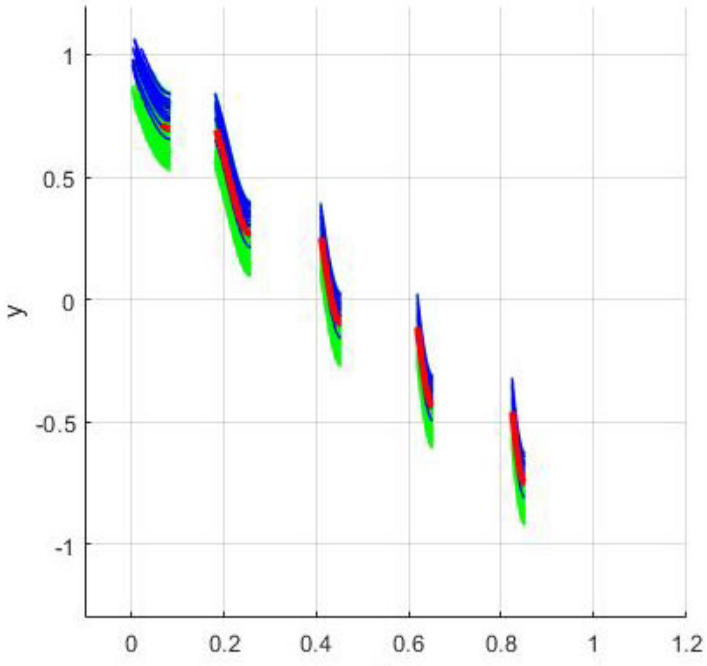

Figure 14: *ZDT3 median Pareto front (red) and confidence interval (green) when the last arc is ignored.*

7 APPLICATION ON A 5-BAR TRUSS STRUCTURE

In this section we study the five-bar truss structure sketched in Figure 15, where we minimize its total mass denoted w, simultaneously with its maximum displacement denoted u (Ellaia et al. 2013). Then we introduce uncertainties on some parameters to see how the solution set behaves when the system values change.

It is assumed that the structure will be modeled by linear, two nodes, bar elements in linear elasticity, subjected only to axial forces and free from imperfections. The geometric and material parameters used are length $l = 9.3144$ m, area $a = 0.01419352$ m^2, load $p = 448.2$ kN, Young$'$s modulus $e = 68.95$ GPa, density $\rho = 2{,}768$ kg/m^3 and yield stress $\bar{\sigma} = 172.4$ MPa.

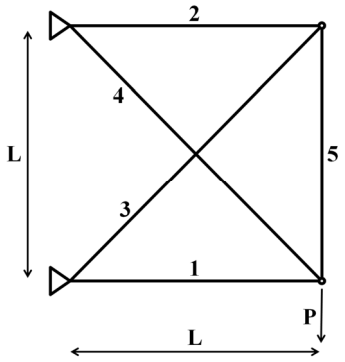

Figure 15: *5 bar truss structure schema*

Denoting $\boldsymbol{x} \in \mathbb{R}^5$ the vector of the topological and sizing optimization parameters, such that $0 \leq x_i \leq 1$ for $i \in \{1, 2, \dots, n\}$ where $n = 5$ is the number of elements, the problem to solve is:

$$\underset{\boldsymbol{x}\in\mathbb{R}^5}{\text{Minimize}} \begin{cases} f_1(\boldsymbol{x}) = w = \sum_{i=1}^{5} \rho\, a l_i x_i \\ f_2(\boldsymbol{x}) = u = \max\left(\boldsymbol{u}^* = \text{argmin}\left(\frac{1}{2}\boldsymbol{u}^t \boldsymbol{k}(\boldsymbol{x})\boldsymbol{u} - \boldsymbol{u}^t \boldsymbol{f}\right)\right) \end{cases} \tag{25}$$

$$\text{Such that}: \sigma_i \leq \bar{\sigma}\,, 1 \leq i \leq n$$

where $\boldsymbol{k}$ is the stiffness matrix and $\boldsymbol{f}$ the vector of loads of the finite element (FE) model and σ_i is the stress of the i^{th} bar.

With a 6 degree polynomial $\boldsymbol{\varphi}$ and $c_{max} = 10$, we get the Pareto front in Figure 16.

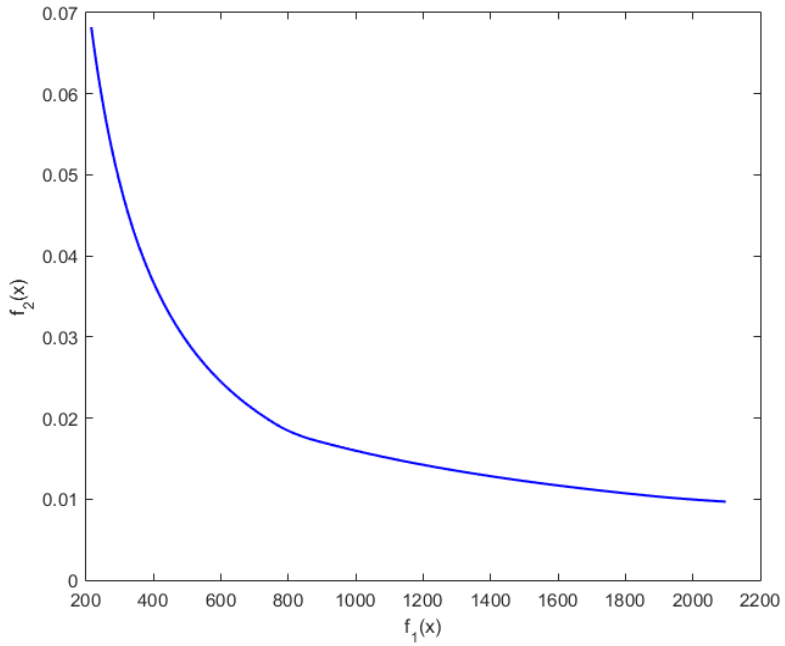

Figure 16: *Pareto front of the 5 bar truss structure*

In the next step we consider:

- the force p that becomes uncertain (denoted P) following a normal distribution with 10% for the coefficient of variation.
- the Young modulus e that becomes uncertain too (denoted E) following a truncated normal distribution defined on $[60.68\ ,\ 77.22]$GPa with 3% for the coefficient of variation.

As done with the test functions, ns $= 200$ problems are generated with a MCS and the result we obtained is shown in Figure 17:

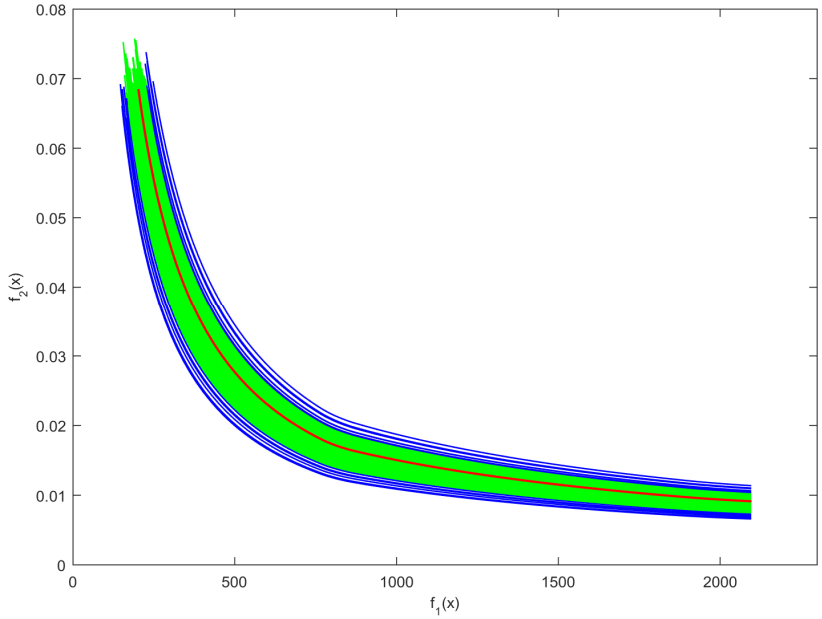

Figure 17: *Pareto fronts of the 5 bar truss structure with uncertainties: the median Pareto front appears in red, the confidence interval in green and the Pareto fronts beyond the 90%-quantile in blue*

In Figure 17, results are "as expected": the mean is in the middle of the curves set, while curves beyond the 90%-quantile (in blue) are located at the exterior of the curves set.

8 Summary

In this work, the MOO problems with constraints and uncertainties are addressed. Instead of analyzing a cloud of data points, the adopted point of view consists of analyzing the randomness of objects that can be modeled by continuous geometric forms, thanks to the Zidani and Souza de Cursi's method which leads to a piecewise continuous Pareto front for the MOO problems, and curves distances measures. Hence, by using a Monte Carlo simulation, a sample of Pareto fronts is generated and the Hausdorff's distance leads to a Pareto front quantile analysis, from the link that we made between Statistics and Geometry. Three academic problems are first modified to handle uncertainties and then solved. Next, an application to a 5-bar truss structure with two exogenous random variables is considered to demonstrate the applicability of the proposed method with a more difficult problem. All results obtained appear satisfactory when observing the location of the median curve and quantiles.

A possible perspective of this work is to apply the approach presented in this paper to a MOO problem under uncertainties where objective functions and constraints are expended with Generalized Fourier Series (Bassi et al. 2016). The use of approximated functions instead of the initial ones aims to reduce the algorithms running time.

Example 6.3 shows that Hausdorff's distance may lead to results that may be considered as unexpected from the eye's point of view. We may find in the literature modifications of Hausdorff's distance (see, for instance, Dubuisson and Jain, 1994) - different distances may be used with the procedure exposed in this work. The comparison between the existing distances and the definition of criteria for the selection of the adequate one will be matter of further work.

References

Amodeo L., Chen H., El Hadji A. (2007), Multi-objective Supply Chain Optimization: An Industrial Case Study. In: Giacobini M. (eds) Applications of Evolutionary Computing. EvoWorkshops 2007. Lecture Notes in Computer Science, vol 4448. Springer, Berlin, Heidelberg

Bachur, W.E. G., Gonçalves, E. N., Ramírez, J. A., Batista, L. S. (2017) A multiobjective robust controller synthesis approach aided by multicriteria decision analysis, Applied Soft Computing, Volume 60, pages 374-386, https://doi.org/10.1016/j.asoc.2017.06.027.

Bassi, M., Souza de Cursi, J. E., Ellaia, R. (2016) Generalized Fourier Series for Representing Random Variables and Application for Quantifying Uncertainties in Optimization, 3rd International Symposium on Uncertainty Quantification and Stochastic Modeling, Maresias, SP, Brazil, February 15-19, 2016

Bawa, V. S. (1975) Optimal rules for ordering uncertain prospects, Journal of Financial Economics, Volume 2, Issue 1, pages 95-121, https://doi.org/10.1016/0304-405X(75)90025-2.

Bawa, V. S. and Goroff, D. L (1983) Stochastic dominance, efficiency and separation in financial markets, Journal of Economic Theory, Volume 30, Issue 2, pages 410-414, https://doi.org/10.1016/0022-0531(83)90115-1.

Binh, T. and Korn, U. (1997) MOBES: A Multiobjective Evolution Strategy for Constrained Optimization Problems. In: Proceedings of the Third International Conference on Genetic Algorithms. Czech Republic, 176-182

Collette, Y. and Siarry, P. (2002) Optimisation multiobjectif, Eyrolles, Paris

Craven, B. D. and Islam, S. M. N. (2005), Optimization in Economics and Finance: Some Advances in Non-Linear, Dynamic, Multi-Criteria and Stochastic Models, Springer, USA

Croquet, R. and Souza de Cursi, E. (2010) Statistics of Uncertain Dynamical Systems, in B.H.V. Topping, J.M. Adam, F.J. Pallarés, R. Bru, M.L. Romero, (Editors), "Proceedings of the Tenth International Conference on Computational Structures Technology", Civil-Comp Press, Stirlingshire, UK, Paper 173, 2010. doi:10.4203/ccp.93.173

Dubuisson, M.-P and Jain, A.K. (1994). A modified Hausdorff distance for object matching. Proceedings of the 12th IAPR International Conference. Vol. 1. 566 - 568 vol.1. 10.1109/ICPR.1994.576361.

Ellaia, R., Habbal, A. and Pagnacco, E. (2013) A New Accelerated Multi-objective Particle Swarm Algorithm: Applications to Truss Topology Optimization, 10th World Congress on Structural and Multidisciplinary Optimization, Orlando, Florida, USA

Fonseca, C. M. and Fleming, P. J. (1995), An overview of evolutionary algorithms in multiobjective optimization, Evolutionary Computation, 3:1: 1-16.

Gass, S. and Saaty, T. (1955), The computational algorithm for the parametric objective function. Naval Research Logistics, 2: 39-45. doi:10.1002/nav.3800020106

Geoffrion, A.M., Dyer, J.S., and Feinberg, A. (1972), An Interactive Approach for Multi-Criterion Optimization, with an Application to the Operation of an Academic Department, Management Science 19, No.4, 357-368.

Hadar, J., Russell, W. (1969). Rules for Ordering Uncertain Prospects. American Economic Review. 59 (1): 25–34.

Haimes, Y.Y., Lasdon, L.S. and Wismer, D.A. (1971) On a Bicriterion Formulation of the Problems of Integrated System Identification and System Optimization, IEEE Transactions on Systems, Man, and Cybernetics 1, 296-297. doi:10.1109/tsmc.1971.4308298

Hurson, Ch and Zopounidis, C. (1997), On The Use Of Multicriteria Decision Aid Methods To Portfolio Selection, Springer, Berlin, Germany

Ivanov, S. Y. and Ray, A. K. (2014), Multiobjective Optimization of Industrial Petroleum Processing Units Using Genetic Algorithms, Procedia Chemistry, 10:2014: 7-14. doi: 10.1016/j.proche.2014.10.003

Ji, R. and Lejeune, M.A. (2018) Risk-budgeting multi-portfolio optimization with portfolio and marginal risk constraints Ann Oper Res 262: 547. https://doi-org.ezproxy.normandie-univ.fr/10.1007/s10479-015-2044-9

Keeney, R.L. and Raiffa, H. (1994) Decisions with multiple objectives–preferences and value tradeoffs, Cambridge University Press, Cambridge & New York, 1993, 569 pages, ISBN 0-521-44185-4 (hardback), 0-521-43883-7 (paperback). Syst. Res., 39: 169-170. doi:10.1002/bs.3830390206

Light, B. (2018) Precautionary saving in a Markovian earnings environment, Review of Economic Dynamics, Volume 29, pages 138-147, https://doi.org/10.1016/j.red.2017.12.004.

Mankiw, N.G. (2011), Principles of Economics - 6th edition, Southwestern College Publishing, Tennessee, USA

Miettinen, K. (1999) Nonlinear multiobjective optimization, Kluwer Academic Publishers, Boston, (1999)

Moreira, F. R., Lobato, F. S., Cavalini Jr, A. A., Steffen Jr, V. (2016). Robust Multi-objective Optimization Applied to Engineering Systems Design. Latin American Journal of Solids and Structures, 13(9), 1802-1822. https://dx.doi.org/10.1590/1679-78252801

Navabi, M. and Mirzaei, H. (2017) Robust Optimal Adaptive Trajectory Tracking Control of Quadrotor Helicopter. Latin American Journal of Solids and Structures, vol.14, no.6, p.1040-1063. http://dx.doi.org/10.1590/1679-78253595

Pätäri, E., Karell, V., Luukka, P., and Yeomans, J. S. (2018), Comparison of the multicriteria decision-making methods for equity portfolio selection: The U.S. evidence, European Journal of Operational Research, 265:2: 655-672. doi: 10.1016/j.ejor.2017.08.001.

Sahinidis, N. V. (2004), Optimization under uncertainty: state-of-the-art and opportunities, Computers and Chemical Engineering, 28: 971–983. doi: 10.1016/j.compchemeng.2003.09.017

Souza de Cursi, E. (2015), Variational Methods for Engineers with Matlab, Wiley

Varian, H. (2006), Microeconomic Analysis, Cram101 Inc., USA

Varian, H. (2009), Intermediate Microeconomics: A Modern Approach, - 8th edition, W. W. Norton & Company

Xidonas, P., Mavrotas, G., Hassapis, C., Zopounidis, C. (2017) Robust multiobjective portfolio optimization: A minimax regret approach, European Journal of Operational Research, Volume 262, Issue 1, pages 299-305, https://doi.org/10.1016/j.ejor.2017.03.041.

Yager, R. R. (2018) Refined expected value decision rules, Information Fusion, Volume 42, pages 174-178, https://doi.org/10.1016/j.inffus.2017.10.008.

Zadeh, L. (1963), Optimality and Non-Scalar Valued Performance Criteria, IEEE Transactions on Automatic Control 8, 59-60. doi:10.1109/tac.1963.1105511

Zidani, H., Ellaia, R., and Souza De Cursi, E. (2013) Representation of solution for multiobjective optimization: RSMO for generating a Su sant Pareto front, Proceedings of 2013 International Conference on Industrial Engineering and Systems Management (IESM), Rabat, 2013, pp. 463-463.

Zitzler, E., Deb, K. and Thiele, L. (2000) Comparison of multi-objective evolutionary algorithms: Empirical results. Evolutionary Computation, 8(2), 173-195, 2000.

Zopounidis, C. (1999), Multicriteria Decision Aid in Financial Management, European Journal of Operational Research, 119:2: 404-415. doi: 10.1016/S0377-2217(99)00142-3.

Appendix A

THE VARIATIONAL APPROACH FOR THE MULTI-OBJECTIVE OPTIMIZATION PROBLEM

In this appendix, we explain the variational approach that leads to the Zidani-Souza's method used in this work, originally proposed in Zidani et al. (2013) and in Souza de Cursi (2015).

Let us consider two objective functions f_1 and f_2 having as individual minima:

$$\begin{cases} \boldsymbol{x_1^*} = \underset{\boldsymbol{x}\in S_d}{\operatorname{argmin}} f_1(\boldsymbol{x}) \\ \boldsymbol{x_2^*} = \underset{\boldsymbol{x}\in S_d}{\operatorname{argmin}} f_2(\boldsymbol{x}) \end{cases} \tag{26}$$

We look for a curve connecting these two points, defined by an unknown vector of parameters $\boldsymbol{c}$:

$$\boldsymbol{x}(\boldsymbol{c},t) = (x_1(\boldsymbol{c},t), x_2(\boldsymbol{c},t), \dots, x_d(\boldsymbol{c},t))^{\mathrm{t}} = (\boldsymbol{x_2^*} - \boldsymbol{x_1^*}).t + \boldsymbol{x_1^*} + \boldsymbol{\varphi}(\boldsymbol{c},t) \tag{27}$$

The variable t is assumed to belong to [0,1]. Since $\boldsymbol{x_1^*}$ and $\boldsymbol{x_2^*}$ belong to the curve, we have:

$$\forall \boldsymbol{c} : \boldsymbol{\varphi}(\boldsymbol{c},0) = \boldsymbol{\varphi}(\boldsymbol{c},1) = \boldsymbol{0} \tag{28}$$

A simple choice consists in using polynomials, such as, for instance

$$\boldsymbol{\varphi}(t) = \sum_{i=1}^{n-1} \boldsymbol{c_{.i}} \left(t^i - 1\right) - \boldsymbol{c_{.n}}(t^n - 1) \text{ with } \boldsymbol{c_{.n}} = \sum_{i=1}^{n-1} \boldsymbol{c_{.i}} \ , \boldsymbol{c_{.i}} \in \mathbb{R}^d \tag{29}$$

where $\boldsymbol{c_{.i}}$ stands for the i$^{\text{th}}$ column of the coefficient matrix $\boldsymbol{c}$.

Taking the last condition into account, we may look for

$$\boldsymbol{\varphi}(t) = \sum_{i=1}^{n-1} \boldsymbol{c_{.i}} \left(t^{i+1} - t^i\right), \boldsymbol{c_{.i}} \in \mathbb{R}^d \tag{30}$$

In order to solve a given MOO problem, let $\boldsymbol{c_{.1}}, \boldsymbol{c_{.2}}, \dots, \boldsymbol{c_{.n}}$ be varying into a set C that we choose in compliance with the situation under consideration. The Pareto front is obtained by minimizing the hypervolume between the curve $\left\{\boldsymbol{p}(c,t) = \left(f_1(\boldsymbol{x}(\boldsymbol{c},t)), f_2(\boldsymbol{x}(\boldsymbol{c},t))\right), t \in [0,1]\right\}$ and the utopia point, or by maximizing the hypervolume between this curve and the anti-utopia point (Figure 18). In this work, we apply the first method by using the Stokes formula that allows the use of the integration on a curve instead of the integration on a surface:

$$A(\boldsymbol{c}) = \int_{t\in[0,1]} \left\langle \mathrm{rot}\left(\boldsymbol{p}(\boldsymbol{c},t)\right) \middle| \nabla \boldsymbol{p}(\boldsymbol{c},t) \right\rangle dt \tag{31}$$

where $\mathrm{rot}(\boldsymbol{p})$ stands for the rotational of $\boldsymbol{p}$. Once we solve the problem:

$$\boldsymbol{c_{sol}} = \underset{C}{\operatorname{argmin}}\, A(\boldsymbol{c}) \tag{32}$$

we get the Pareto front S_{sol} of $\mathbb{R}^2$ as:

$$S_{sol} = \left\{\boldsymbol{p}^*(c,t) = \left(f_1(\boldsymbol{x}(\boldsymbol{c_{sol}},t)), f_2(\boldsymbol{x}(\boldsymbol{c_{sol}},t))\right), t \in [0,1]\right\} \tag{33}$$

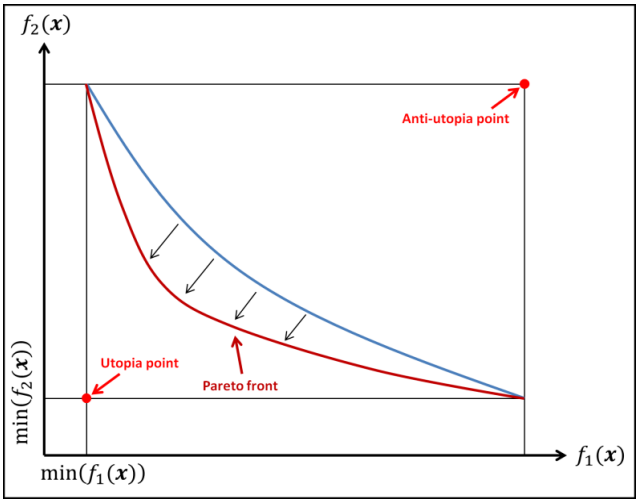

Figure 18: *Pareto front using Zidani-Souza's method*